

DECIPHERING THE 3D STRUCTURE OF THE OLD GALACTIC BULGE FROM THE OGLE RR LYRAE STARS

P. PIETRUKOWICZ¹, S. KOZŁOWSKI¹, J. SKOWRON¹, I. SOSZYŃSKI¹, A. UDALSKI¹, R. POLESKI^{1,2}, Ł. WYRZYKOWSKI^{1,3},
M. K. SZYMAŃSKI¹, G. PIETRZYŃSKI^{1,4}, K. ULACZYK¹, P. MRÓZ¹, D. M. SKOWRON¹, AND M. KUBIAK¹

¹ Warsaw University Observatory, Al. Ujazdowskie 4, 00-478 Warszawa, Poland

² Department of Astronomy, Ohio State University, 140 W. 18th Ave., Columbus, OH 43210, USA

³ Institute of Astronomy, University of Cambridge, Madingley Road, Cambridge CB3 0HA, UK

⁴ Universidad de Concepción, Departamento de Física, Casilla 160-C, Concepción, Chile

Received 2014 December 12; accepted 2015 August 24; published 2015 September 28

ABSTRACT

We have analyzed a sample of 27,258 fundamental-mode RR Lyrae variable stars (type RRab) detected recently toward the Galactic bulge by the Optical Gravitational Lensing Experiment (OGLE) survey. The data support our earlier claim that these metal-poor stars trace closely the barred structure formed of intermediate-age red clump giants. The distance to the Galactic center (GC) inferred from the bulge RR Lyrae stars is $R_0 = 8.27 \pm 0.01(\text{stat}) \pm 0.40(\text{sys})$ kpc. We show that their spatial distribution has the shape of a triaxial ellipsoid with a major axis located in the Galactic plane and inclined at an angle of $i = 20^\circ \pm 3^\circ$ to the Sun–GC line of sight. The obtained scale-length ratio of the major axis to the minor axis in the Galactic plane and to the axis vertical to the plane is 1:0.49(2):0.39(2). We do not see evidence for the bulge RR Lyrae stars forming an X-shaped structure. Based on the light curve parameters, we derive metallicities of the RRab variables and show that there is a very mild but statistically significant radial metallicity gradient. About 60% of the bulge RRab stars form two very close sequences on the period–amplitude (or Bailey) diagram, which we interpret as two major old bulge populations: A and B. Their metallicities likely differ. Population A is about four times less abundant than the slightly more metal-poor population B. Most of the remaining stars seem to represent other, even more metal-poor populations of the bulge. The presence of multiple old populations indicates that the Milky Way bulge was initially formed through mergers.

Key words: Galaxy: bulge – Galaxy: structure – stars: variables: RR Lyrae

1. INTRODUCTION

RR Lyrae type variable stars are well-known tracers of old and metal-poor populations. They play an essential role in the understanding of the structure, formation, and evolution of the Milky Way. Multi-epoch observations allow easy identification of this type of variable, in particular of high-amplitude fundamental-mode RRab type stars with characteristic tooth-shaped light curves. Based on a large number of observations one can determine their properties with high precision, such as period, metallicity, interstellar reddening, distance, and spatial distribution.

Thousands of RR Lyrae stars have been discovered in the Galactic bulge, thick disk, and halo. Observations of the halo variables (e.g., Kinemuchi et al. 2006; Keller et al. 2008; Sesar et al. 2010; Akhter et al. 2012; Mateu et al. 2012; Süveges et al. 2012; Drake et al. 2013; Zinn et al. 2014; Torrealba et al. 2015) indicate that it probably consists of two overlapping populations (Miceli et al. 2008; Szczygieł et al. 2009) and is full of substructures from tidally disrupted dwarf galaxies such as the Sagittarius dwarf spheroidal (Sgr dSph) galaxy (Cseresnjes 2001; Kunder & Chaboyer 2009; Torrealba et al. 2015).

Central regions of the Milky Way have been intensively monitored by the Optical Gravitational Lensing Experiment (OGLE) since the early 1990s (Udalski et al. 1992). Since 2010 March the project has been in its fourth phase (OGLE-IV, Udalski et al. 2015). With the survey area increasing in each of the previous phases, the number of detected RR Lyrae variables toward the Galactic bulge has increased significantly: 215 stars in OGLE-I (e.g., Udalski et al. 1997), 2713 stars in OGLE-II (Mizerski 2003), and 16,836 stars in OGLE-III (Soszyński

et al. 2011). The OGLE-III collection consisted of 11,756 fundamental-mode (RRab), 4989 first-overtone (RRc), and 91 double-mode (RRd) stars. The analysis of that sample by Pietrukowicz et al. (2012) showed that the bulge RR Lyrae stars seem to constitute a uniform population with a sharply peaked metallicity distribution centered at $[\text{Fe}/\text{H}] = -1.02 \pm 0.18$ dex on the Juressik (1995) metallicity scale. A comparison of the distributions of the dereddened brightnesses of RR Lyrae stars and red clump (RC) giants indicated that in the inner regions ($|l| < 3^\circ, |b| < 4^\circ$) the RR Lyrae stars tend to follow the barred structure of RC stars inclined at an angle of about 30° with respect to the line of sight between the Sun and the Galactic center (GC) (Rattenbury et al. 2007; Gonzalez et al. 2011; Cao et al. 2013; Nataf et al. 2013; Wegg & Gerhard 2013; Bobylev et al. 2014).

Dékány et al. (2013) combined I -band OGLE measurements with near-IR K_s -band data from the VISTA Variables in the Via Lactea (VVV) survey (Minniti et al. 2010) for 7663 OGLE-III RRab variables in order to refine the spatial distribution of the old bulge population. These authors claim that the population of RR Lyrae stars has a nearly spherical distribution, slightly elongated in its central part almost toward us. They obtained a distance to the GC of $R_0 = 8.33 \pm 0.05(\text{stat}) \pm 0.14(\text{sys})$ kpc and an inclination angle of $12.5^\circ \pm 0.5^\circ$.

Very recently, Soszyński et al. (2014) presented a collection of 38,257 RR Lyrae variable stars detected in the OGLE fields covering over 182 deg^2 of the central regions of the Galactic bulge. In this set, 21,453 RR Lyrae stars are newly discovered objects in OGLE-IV. The collection consists of 27,258 RRab, 10,825 RRc, and 174 RRd stars. In this paper, we study the spatial structure of the old Galactic bulge based on the whole

available sample of the detected RRab type stars from the OGLE survey. Variables of this type are on average brighter, have higher amplitudes, and thanks to their characteristic saw-tooth-shaped light curves are hard to overlook in comparison to first-overtone sinusoidal-like RRc pulsators.

We also use the new large sample of RRab type variables to investigate population properties of the Milky Way old bulge. In early studies, classical bulges were assumed to be characterized by single stellar populations whose stars formed on short timescales (e.g., Hernquist 1990; Trager et al. 2000). However, modern spectroscopic studies have revealed a more complex picture of star formation history via collapse, mergers, and secular processes (e.g., Moorthy & Holtzman 2006; Morelli et al. 2008; Seidel et al. 2015). RR Lyr stars as tracers of old populations may help to identify the dominant mechanism responsible for the early formation of our Galaxy.

The outline of this paper is as follows. Section 2 describes the cleaning procedure of the sample. In Section 3, we analyze the observed distribution of the bulge RRab stars on the sky. The analysis of the spatial structure is included in Section 4. In Section 5, we investigate the photometric metallicity gradient. In Section 6, we present the discovery of multiple old populations among the bulge RR Lyrae stars. Finally, Section 7 states the main conclusions of this work.

2. DATA SAMPLE

Prior to the analysis of the bulge RR Lyrae stars the original sample from Soszyński et al. (2014) required several cleaning steps. From the whole sample of 27,258 RRab variables, we rejected 54 stars as being bona fide members and very likely members of eight globular clusters (NGC 6441, NGC 6522, NGC 6540, NGC 6553, NGC 6558, NGC 6569, NGC 6642, and NGC 6656). This procedure was based on Clement et al.’s (2001) catalog of variable stars in Galactic globular clusters and its 2010 update.⁵ From the original list, we also rejected object OGLE-BLG-RRLYR-02792 which was recently confirmed to be a low-mass binary component mimicking an RR Lyrae pulsator (Pietrzyński et al. 2012; Smolec et al. 2013).

In the next step, we cleaned the bulge sample from foreground and background RR Lyrae stars by constructing the color-magnitude ($V - I$, I) diagram (upper panel in Figure 1). Due to different reddening toward observed regions the bulge stars form a long sequence in the diagram. By drawing three lines we roughly delimited bulge RR Lyrae variables from background stars (line at $I = 1.1(V - I) + 16.0$), foreground stars (line at $I = 1.1(V - I) + 13.0$), and stars with unreliable color (vertical line at $V - I = 0.3$ mag). Most of the background objects are variables from the Sgr dSph galaxy. Other background variables and all foreground variables very likely belong to the Milky Way thick disk and halo. Binning of the bulge data shows that the sequence is clearly linear for $0.7 < V - I < 3.1$ mag (lower panel in Figure 1) and can be described with the following relation:

$$I = 1.144(9)(V - I) + 14.432(18), \quad (1)$$

where its slope is the total-to-selective extinction $R_{I,V-I} = A_I/E(V - I)$. It is 0.06 higher than the one found based on a sample from the OGLE-III data that was a factor of two smaller (Pietrukowicz et al. 2012). The obtained value

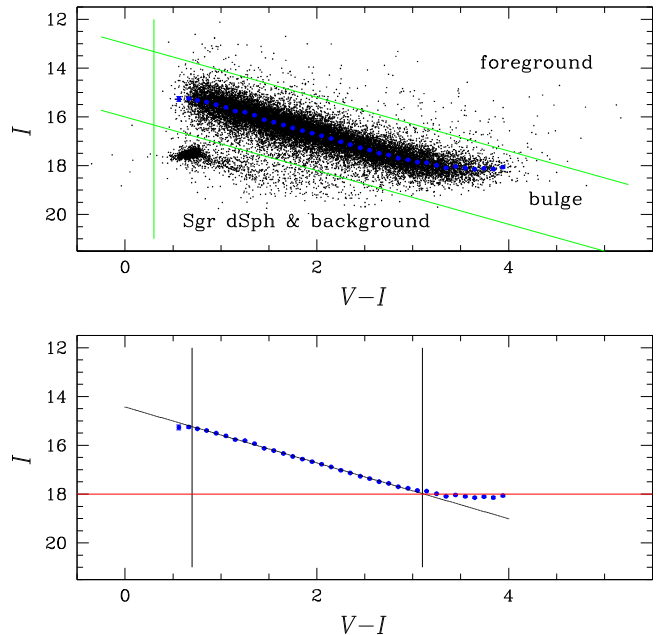


Figure 1. Color-magnitude diagram (based on mean values) for all 27,258 RRab variables observed in the OGLE fields (upper panel). Candidate bulge variables are located inside the three green lines. Other stars are very likely foreground and background objects. The lower sequence is formed by variables from the Sgr dSph galaxy. Binning of the bulge data every 0.1 mag in the $V - I$ color (blue points) shows that the bulge sequence is practically linear for $0.7 < V - I < 3.1$ mag and complete down to $I = 18.0$ mag (lower panel).

of $R_{I,V-I}$ is consistent with the fact that the interstellar extinction toward the bulge is anomalous (Udalski 2003; Nataf et al. 2013).

The mean brightness of the bulge sequence clearly departs from linear at $I \sim 18$ mag or $V - I \sim 3.1$ mag. Hence, we assume that our sample of RRab stars is complete down to $I = 18.0$ mag. The total number of bulge variables with measured mean brightnesses in V and I amounts to 21,026 objects.

In Figure 2, we show a map with positions in Galactic coordinates of all OGLE RR Lyrae variables with available VI data and distinguish between stars brighter and fainter than $I = 18.0$ mag. These stars concentrate toward the GC, but due to high extinction they are not observed in the optical regime close to the Galactic plane. By drawing two lines we set borders of two areas, north and south of the plane, in which, as we assume, all bulge RRab stars have been detected within the OGLE bulge fields. In our analysis of the old bulge structure, we rely only on objects from the “complete” directions. The whole “complete” area amounts to 90.5 deg^2 .

3. DISTRIBUTION ON THE SKY

Based on the OGLE-III data Pietrukowicz et al. (2012) evidently confirmed an earlier finding by Minniti et al. (1998) that the bulge RR Lyrae population is flattened along Galactic longitude. From the difference in longitudinal and latitudinal surface density profiles, Pietrukowicz et al. (2012) derived an axis ratio of ~ 0.75 . For the present “complete” area covering 50% of the sky within an angular radius of $5^\circ 5$ around the GC and 28% within $8^\circ 75$, we can carry out a more accurate determination of the observed on the sky shape of the old bulge.

⁵ <http://www.astro.utoronto.ca/clement/read.html>

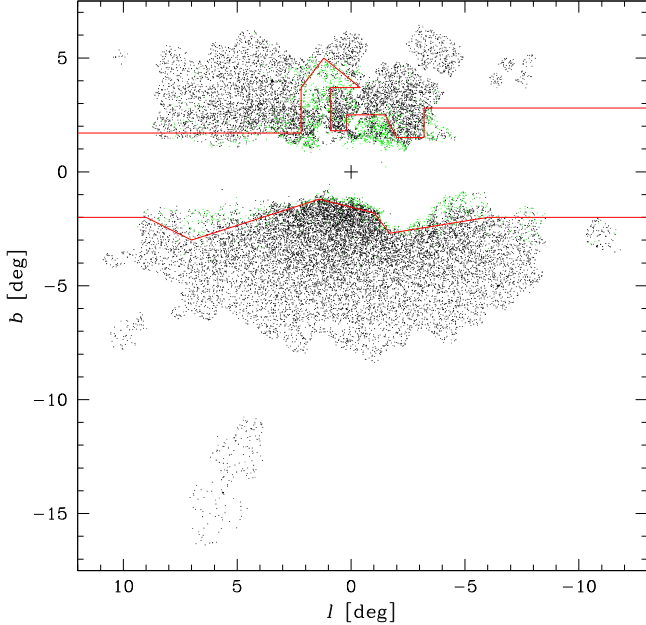


Figure 2. Positions, in Galactic coordinates, of 21,026 OGLE bulge RRab variables with measured brightnesses in both V and I band. Black points are stars with a mean brightness of $I \leq 18$ mag, while green ones are those with a mean brightness of $I > 18$ mag. Red lines are limits between “complete” areas, toward which, as we assume, all RRab stars have been detected (north of the upper line and south of the lower one) and an “incomplete” stripe along the Galactic plane due to high extinction.

We counted stars in cells in a radial coordinate system around $(l, b) = (0, 0)$. The cells were spaced every 15° in azimuth and they were $0^\circ.75$ long in radius. We sampled every $0^\circ.05$ in radial distance between $1^\circ.25$ and $8^\circ.0$ from the center. The density in each cell was corrected for surface coverage. Cells covering less than 80% of the “complete” directions were not taken into account. Results of the surface density determination are presented in Figure 3, where centers of the cells are represented by points in five different colors. The colors code five density ranges. To the points from the same density range we fitted ellipses with the centers on the Galactic equator and described by the semimajor axis r_l and semiminor axis r_b . The obtained flattening $f = 1 - r_b/r_l$ in a function of r_l is plotted in the inset of Figure 3. It does not seem to change with increasing distance, hence we assume it to be constant at a mean value of 0.33 ± 0.03 .

The most important implication from the observed surface density distribution of the RR Lyrae stars is that the old bulge is not spherically symmetric—it is ellipsoidal.

The uncertainty of the flattening $\sigma_f = 0.03$ is much larger than the effects of spherical projection. These effects are comparable to the obtained σ_f at a distance of about 30° . They are negligible at radial distances up to 10° from the center.

In two panels of Figure 4, we present the radial surface density profile for the bulge RRab stars. We counted stars in equally spaced annuli in a logarithmic angular distance scale from the center at $(l, b) = (0, 0)$. The data were corrected for completeness and scaled to the minor (vertical) axis r_b (r_Z) by the factor $r_b/r_l = 0.67$. In the upper panel, we show the results in units of degrees, while in the lower one, we convert the units of degrees to kiloparsecs by adopting the distance to the GC obtained further in Section 4, $R_0 = 8.27$ kpc. The OGLE data span angular distances between $1^\circ.5$ and $19^\circ.9$ or linear

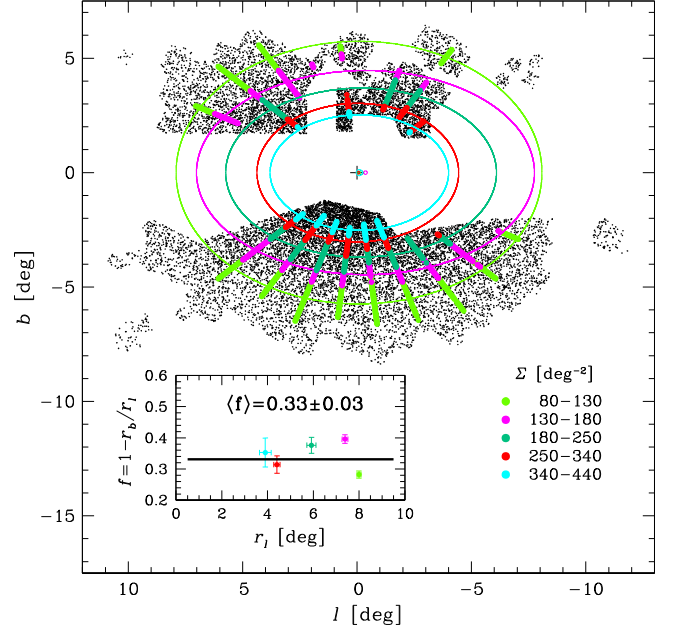


Figure 3. Observed surface density of the bulge RRab stars determined in “complete” directions up to 8° from the Galactic center. Constant density lines are ellipses with the major axis along the Galactic equator. Their centers are marked with small circles representing the uncertainty. The observed semiminor to semimajor axis ratio r_b/r_l does not seem to change with the distance from the center. The projected flattening $f = 1 - r_b/r_l$ has a mean value of 0.33 ± 0.03 (inset).

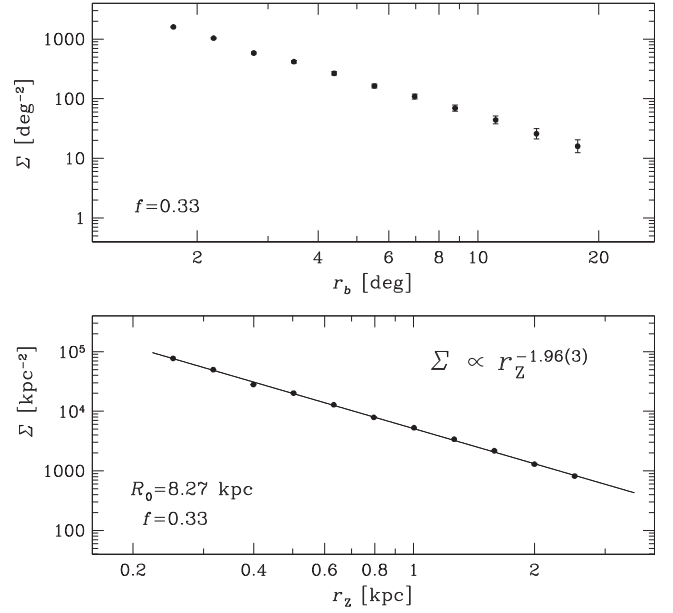


Figure 4. Radial surface density profile of RRab stars calculated for the observed flattening f and scaled to the minor axis in units of degrees (upper panel) and kpc (lower panel) assuming the distance to the Galactic center R_0 determined in Section 4. The obtained profile is a power law within the whole observed distance range from the center.

distances from about 0.22 to 2.8 kpc from the GC. As one can see, the surface density profile of RRab stars in this Galactocentric distance range can be represented by a single power law:

$$\log \Sigma = -1.96(3) \log r_Z + 3.709(14). \quad (2)$$

This result is much more precise than the one presented in Pietrukowicz et al. (2012) where the sky coverage and the RRab sample were significantly smaller and variables were counted in OGLE-III fields as units. Here we see that there is no break in the density distribution at a distance of 0.5 kpc from the GC as reported in earlier work.

4. THE 3D STRUCTURE

4.1. Calculation of the Distances to the RR Lyrae Stars

In this section, we derive parameters describing the spatial structure of the RR Lyrae population. To obtain distances to individual stars we have to correct their brightness for reddening. We calculated dereddened mean magnitudes using

$$I_0 = I - A_I, \quad (3)$$

where the extinction A_I was derived from the following formula introduced in Nataf et al. (2013):

$$A_I = 0.7465E(V-I) + 1.3700E(J-K). \quad (4)$$

The reddening in the optical regime is

$$E(V-I) = (V-I) - (V-I)_0, \quad (5)$$

where the intrinsic color

$$(V-I)_0 = M_V - M_I. \quad (6)$$

In Equation (6), the absolute brightnesses M_V and M_I were computed from the theoretical relations given in Catelan et al. (2004):

$$M_V = 2.288 + 0.882 \log Z + 0.108 (\log Z)^2, \quad (7)$$

$$M_I = 0.471 - 1.132 \log P + 0.205 \log Z, \quad (8)$$

with the following conversion for metallicity:

$$\log Z = [\text{Fe}/\text{H}] - 1.765. \quad (9)$$

The zero points of the relations for M_V and M_I were calibrated to the data obtained for the well-studied representative globular cluster M3 (NGC 5272, Catelan 2004), which hosts about 240 RR Lyrae variables (Clement et al. 2001). We measured the metallicities on the Juresik (1995) scale (J95) by applying an empirical relation from Smolec (2005):

$$[\text{Fe}/\text{H}]_{\text{J95}} = -3.142 - 4.902P + 0.824\phi_{31}, \quad (10)$$

where P is the pulsation period and $\phi_{31} = \phi_3 - 3\phi_1$ is a Fourier phase combination for sine decomposition of the I -band light curve. The reddening $E(J-K)$ was taken from the maps in Gonzalez et al. (2012) which were prepared in the framework of the VVV survey (Minniti et al. 2010). It is available for RR Lyr stars located within the VVV bulge area of the following limits: $-10^\circ 1 \leq l \leq 10^\circ 4$ and $-10^\circ 4 \leq b \leq +5^\circ 1$.

Finally, the distance d to each RRab stars was calculated from the equation

$$d = 10^{1+0.2(I_0-M_I)}. \quad (11)$$

4.2. Distance to the GC

Having distances to individual RR Lyrae stars we can estimate the distance to the center of the entire old population, which we assume to coincide with the center of our Galaxy.

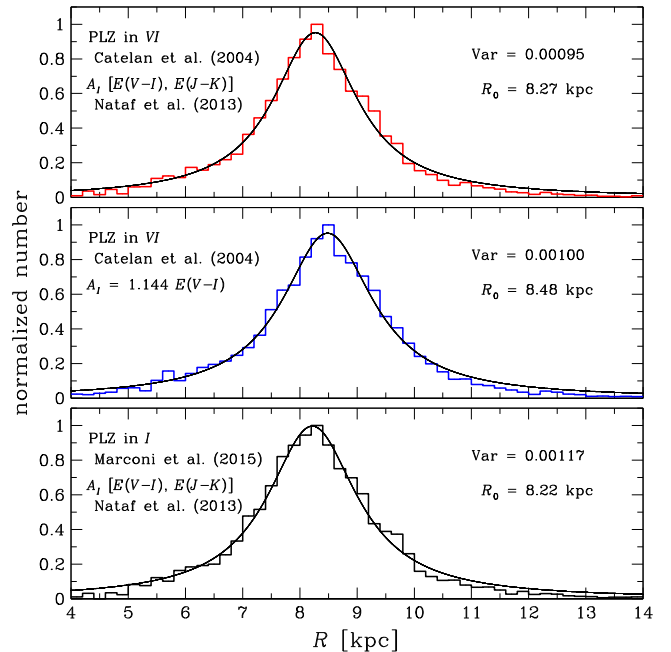


Figure 5. Distance distribution for RRab stars from an area with Galactic coordinates $-4^\circ < l < +4^\circ$ and $-6^\circ 7 < b < -2^\circ 7$ obtained with three different methods: using theoretical period–luminosity–metallicity (PLZ) relations in the VI bands from Catelan et al. (2004) and Nataf et al. (2013) for extinction with optical and near-IR components (upper panel), using theoretical relations also from Catelan et al. (2004) but with a simple linear correction for absorption with the total-to-selective extinction $R_{I,V-I} = 1.144$ (middle panel), and by applying a theoretical period–luminosity–metallicity relation in the I band from Marconi et al. (2015) and the formula for extinction from Nataf et al. (2013) (lower panel). The first method gives the smallest variance of residuals and a maximum value at $R_0 = 8.27$ kpc, which is the closest to the most recent estimates of the distance to the Galactic center of about 8.3 kpc. The third method leads independently to very similar distance estimates.

Inside the “complete” OGLE directions, we selected a rectangle area symmetric in Galactic longitude with $-4^\circ < l < +4^\circ$ and $-6^\circ 7 < b < -2^\circ 7$. In the upper panel of Figure 5, we plot the distribution of the distances to 4689 stars from this area calculated using the relation on extinction from Nataf et al. (2013). To the distribution we fit a King (1962)-like profile:

$$n = \frac{n_0}{1 + \left(\frac{d - R_0}{r_c} \right)^2}, \quad (12)$$

where n_0 is the maximum number of stars at distance R_0 , and r_c is the core radius. It is important to note that prior to the fitting we applied two geometric corrections to the data. First, the individual distances were projected onto the Galactic plane (by $\cos b$). Second, we scaled the distribution by d^{-2} to correct for the so-called cone effect where more objects are seen at larger distances inside a solid angle. The maximum of the distribution is at a distance $R_0 = 8.27$ kpc. The obtained value is close to the most recent determinations of the distance to the GC: $8.28 \pm 0.15(\text{stat}) \pm 0.29(\text{sys})$ kpc (Gillessen et al. 2009), 8.27 ± 0.29 kpc (Schönrich 2012), $8.33 \pm 0.05(\text{stat}) \pm 0.14(\text{sys})$ kpc (Dékány et al. 2013), 8.34 ± 0.16 kpc (Reid et al. 2014), $8.27 \pm 0.09(\text{stat}) \pm 0.1(\text{sys})$ kpc (Chatzopoulos et al. 2015).

For a comparison, in the remaining two panels of Figure 5, we show distance distributions obtained in two other ways. In

the middle panel, we apply a simple correction for reddening by taking the mean value of $R_{I,V-I} = 1.144$ determined earlier in Section 2—as was done in Pietrukowicz et al. (2012). In the lower panel, we calculate the distances through a period–luminosity–metallicity relation in the I band for RRab stars provided by Marconi et al. (2015) in their Table 6:

$$M_I = -0.07 - 1.66 \log P + 0.17[\text{Fe}/\text{H}]_{\text{C09}}, \quad (13)$$

where the metallicity is on a scale for globular clusters (Carretta et al. 2009, C09). In this approach, we transformed the metallicities of bulge variables from the J95 scale to C09 via the Zinn & West (1984) scale (ZW84) using a relation from Papadakis et al. (2000):

$$[\text{Fe}/\text{H}]_{\text{ZW84}} = 1.028[\text{Fe}/\text{H}]_{\text{J95}} - 0.242 \quad (14)$$

and the following formula from Carretta et al. (2009):

$$[\text{Fe}/\text{H}]_{\text{C09}} = 1.105[\text{Fe}/\text{H}]_{\text{ZW84}} + 0.160. \quad (15)$$

Here we also use Nataf et al.’s (2013) formula for extinction with $E(J - K)$ from VVV maps in Gonzalez et al. (2012) and $E(V - I)$ from OGLE-III maps in Nataf et al. (2013), in both cases determined from RC giants. As one can see from Figure 5, the method based on theoretical relations from Catelan et al. (2004) and the formula for extinction from Nataf et al. (2013) gives the lowest variance of residuals of the fit and an R_0 closest to the most recent estimates of the distance to the GC. The approach with a non-standard but constant-in-all-directions value of $R_{I,V-I}$ gives a variance of the residuals that is higher by about 5% and a larger value of R_0 . The third method, which relies on an independent set of stellar models, is in very good agreement with our first approach. This shows that both methods are solid. If the reddening maps covered the whole OGLE-IV bulge area, the approach via Marconi et al.’s (2015) PLZ relation could be used for the whole set of RRab stars.

The statistical uncertainty of the distance to the GC based on thousands of RR Lyrae stars is expected to be small. If we adopt a mean accuracy of OGLE brightness measurements at a level of $\sigma_I = \sigma_V = 0.02$ mag (Udalski et al. 2008), an accuracy of the derived metallicity of 0.005 dex at $[\text{Fe}/\text{H}]_{\text{J95}} = -1.02$ dex, and a mean accuracy of the reddening $E(J - K)$ of 0.104 mag, we find a mean uncertainty of the distance modulus to the individual stars of 0.147 mag, and hence an uncertainty of the distance of $\sigma = 0.56$ kpc. The selected rectangle area contains $n = 4689$ variables, which gives a final statistical error of the distance to the GC $\sigma_{R0,\text{stat}} = \sigma/\sqrt{n} = 0.008$ kpc.

The systematic error of R_0 relies on several estimations. In particular, it relies on the quality of estimation of the absolute brightness M_V derived from the luminosity–metallicity dependence. It does not exceed $\Delta M_V = 0.1$ mag if one compares quadratic formulae from Catelan et al. (2004), Sandage & Tammann (2006), and Bono et al. (2007) for metallicities around $[\text{Fe}/\text{H}]_{\text{J95}} = -1.0$ dex. The relation for extinction A_I (Equation (4)) is based on RC giants for which the intrinsic colors are known to an accuracy of $\Delta(V - I)_{\text{RC},0} = 0.01$ mag and $\Delta(J - K)_{\text{RC},0} = 0.02$ mag (Gonzalez et al. 2012; Nataf et al. 2013). This gives an error of $\Delta A_I = 0.028$ mag. The uncertainty of the metallicity relation (Equation (9)) of 0.18 dex (Smolec 2005) propagates to a small additional error of 0.014 mag in the $(V - I)_0$ color of RR Lyrae stars. If we take into account all of the above errors in the equation for the

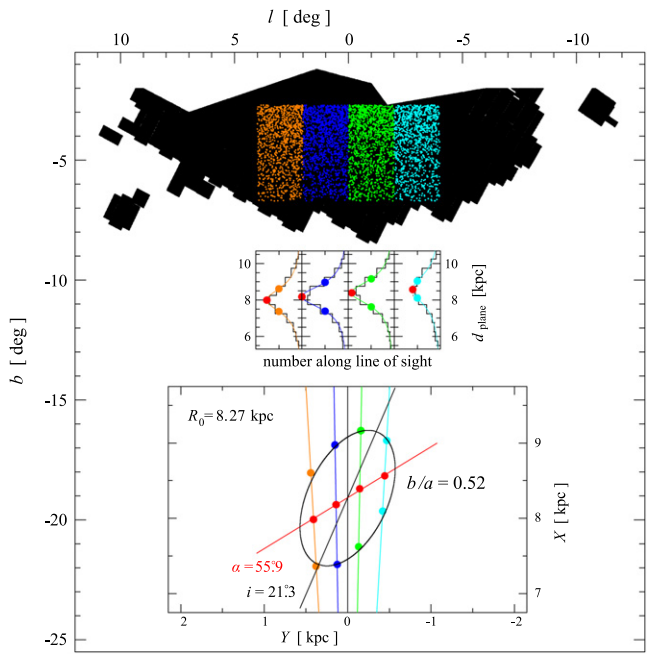


Figure 6. Results from the analysis of the number density distribution of bulge RRab stars along four selected directions. The centers of the four analyzed rectangular areas, shown with different colors, have the same Galactic latitude of $b = -4^\circ 7$ and are equally spaced in Galactic longitude from $l = -3^\circ$ to $l = +3^\circ$. The inset in the middle presents the obtained density distributions. The maxima of the distributions, marked with red dots, clearly change with Galactic longitude. Four pairs of dots represent the same density level in the four investigated directions. In the projection onto the Galactic plane (lower inset), they form an ellipse tilted at an angle of $i \approx 21^\circ$ to the Sun–GC line and the axis ratio $b/a \approx 0.52$. A value of $R_0 = 8.27$ kpc was applied. The Sun is located at $(X, Y) = (0, 0)$.

distance modulus:

$$\mu = I - A_I - M_V + (V - I)_0, \quad (16)$$

we find $\sigma_{\mu,\text{sys}} = 0.105$ mag and hence the systematic uncertainty of the distance to GC of $\sigma_{R0,\text{sys}} \sim 0.40$ kpc. Finally, we have $R_0 = 8.27 \pm 0.008(\text{stat}) \pm 0.40(\text{sys})$ kpc. As expected, the uncertainty of R_0 is dominated by systematic error, whereas the large number of variables significantly lowers the statistical one.

4.3. Geometry of the Old Bulge

To find the shape of the old bulge we use stars from the same rectangular area. We divide the area into four parts equal in longitude as shown with different colors in the upper part of Figure 6. The parts from lower to higher longitude (from right to left) contain 1060, 1292, 1295, and 1042 objects, respectively. For each part, separately, we plot the distance distribution and fit the King-like profile, as presented in the middle part of Figure 6. The colors remain the same for each of the four probed sightlines, associated with the weighted centers of the divided parts. We mark the maxima of the fits with red dots. It is clearly seen that the distance to the maximum decreases with increasing Galactic longitude. In the projection onto the Galactic plane, the maxima form a line tilted at a relatively high angle of about 56° with respect to the Sun–GC line, as illustrated in the lower part of Figure 6. The line for the highest density is not straight but slightly curved, as shown in an auxiliary figure, Figure 7, and cannot be interpreted as the

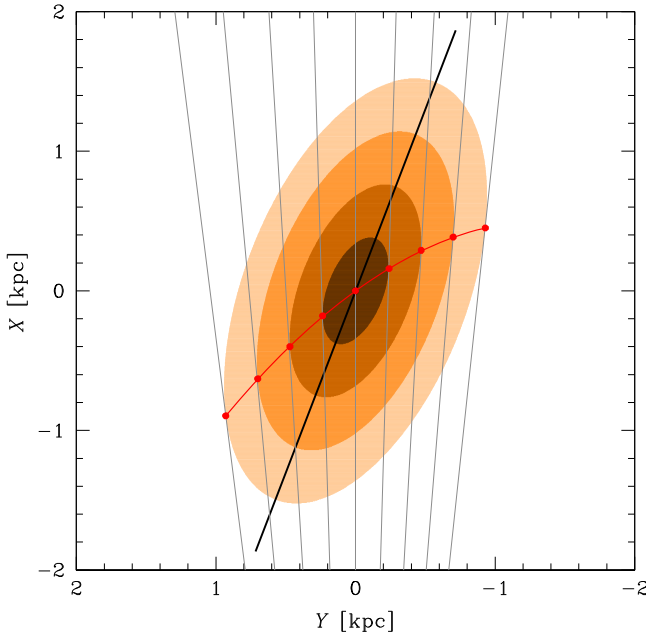


Figure 7. Central part of the Galactic bulge, presented schematically, as it would be seen from the Galactic pole (the one at the positive Galactic latitude). We generate four constant density ellipses with $b/a = 0.5$ inclined at 21° to the line of sight of the observer located at $(Y, X) = (0, -8.27)$ kpc. The black thick line shows the real orientation of the bar’s long axis. The tangential lines (in gray) to the ellipses, starting from the observer, show the points of highest stellar density along these observer lines of sight (red points). The highest density points are often incorrectly interpreted as coinciding with the long axis of the bar, resulting in a wrong, overestimated angle of the bar (see red vs. black lines in the lower inset in Figure 6).

bar’s long axis. To find the true shape and inclination angle of the old bulge, along the four sightlines we mark positions at the same density level, here set at half maximum of the distribution toward $(l, b) = (-1^\circ, -4^\circ.7)$. As one can see, such points form an ellipse with an axis ratio of $b/a \approx 0.52$ tilted at an angle of $i \approx 21^\circ$ to the Sun–GC line. This demonstrates that the old bulge traced by the RR Lyrae stars is a triaxial ellipsoid with major axis a and minor axis b located in the Galactic plane and axis c perpendicular to it.

In the next step, we probe the same area in the sky but for more directions and a wider range of density levels. We selected 13 directions between Galactic longitudes $l = -3^\circ.0$ and $l = +3^\circ.0$ every $0^\circ.5$ at the same latitude $b = -4^\circ.7$. The data were taken in a rectangular box of the same size, 2° wide in longitude and 4° high in latitude, and projected onto the Galactic plane, as done above. To each of 11 density levels we fit an ellipse with the center at $(X, Y) = (8.27, 0)$ kpc and described by the semimajor axis a , axis ratio b/a , and inclination i . Results of the χ^2 minimization of these three parameters are presented in Figure 8. Both the inclination angle and axis ratio are practically constant in the range of probed distances from the center between 0.9 and 1.7 kpc. We find $i = 20^\circ \pm 3^\circ$ and $b/a = 0.490 \pm 0.025$. Closer to the center we obtain different values. In particular, the tilt angle increases up to about 30° . We suspect that the results for the inner part are affected by an ellipse of similar size to that used to bin the data. The angle and axis ratio probably stay the same toward the center. However, we cannot rule out a possibility that they are different.

Knowing the observed flattening on the sky f , axis ratio b/a , and inclination angle i , we can estimate the axis ratio

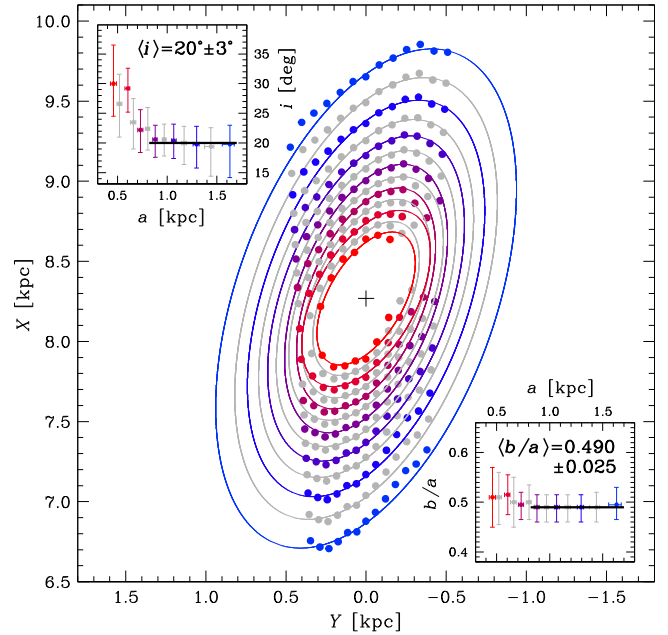


Figure 8. Elliptical density contours fitted to the data along 13 sightlines, from $l = -3^\circ$ to $l = +3^\circ$ every $\Delta l = 0^\circ.5$ and projected onto the Galactic plane. The Sun is located at $(X, Y) = (0, 0)$. For clarity, every other density level is shown in gray. The insets present the obtained inclination angle i (upper left) and axis ratio b/a (lower right) as a function of the semimajor axis a of the ellipse. Ellipses fitted to points at distances 0.9–1.7 kpc have almost the same inclination angle and axis ratio: $i \approx 20^\circ$ and $b/a \approx 0.49$. Closer to the center, our results are likely biased by the size of the data bin (2° in longitude) which is comparable to the size of the ellipse. Both parameters of the ellipse probably stay the same.

c/a of the old bulge ellipsoid (see the appendix). For $f = 0.33 \pm 0.03$, $b/a = 0.490 \pm 0.025$, and $i = 20^\circ \pm 3^\circ$ we find $c/a = 0.384 \pm 0.015$ with the uncertainty returned from Monte Carlo simulations.

At the end of Section 3, we showed that for RRab variables the surface density profile along the vertical axis r_Z can be described as a single power law. Since the positions on the sky are much more accurate than distances to the stars and the Z axis is the true minor axis of the ellipsoid, from the surface density profile we can easily find the spatial density distribution as

$$\log \rho = -2.96(3) \log r_Z + 1.8545(7), \quad (17)$$

with ρ in kpc^{-3} . The obtained power-law index of -2.96 ± 0.03 is comparable to the value of -2.78 ± 0.02 reported for the inner halo RR Lyrae variables in Akhter et al. (2012) and -2.8 for halo main sequence stars near the turn-off point determined by Jurić et al. (2008). This result supports an idea that the old bulge and halo form a uniform Galactic component.

4.4. Absence of an X-shaped Structure in RR Lyrae Stars

With the present sample of OGLE RR Lyrae variables, we can verify whether they follow the same spatial structure in regions where the bulge RC giants show a split in brightness (Nataf et al. 2010) and form an X-shaped bulge (McWilliam & Zoccali 2010). The difference in the I band for RC stars reaches about 0.5 mag at Galactic latitudes $|b| \sim 5^\circ.5$. In Figure 9, we plot histograms of dereddened I -band brightness derived for two sets of RRab stars, both for objects with latitudes

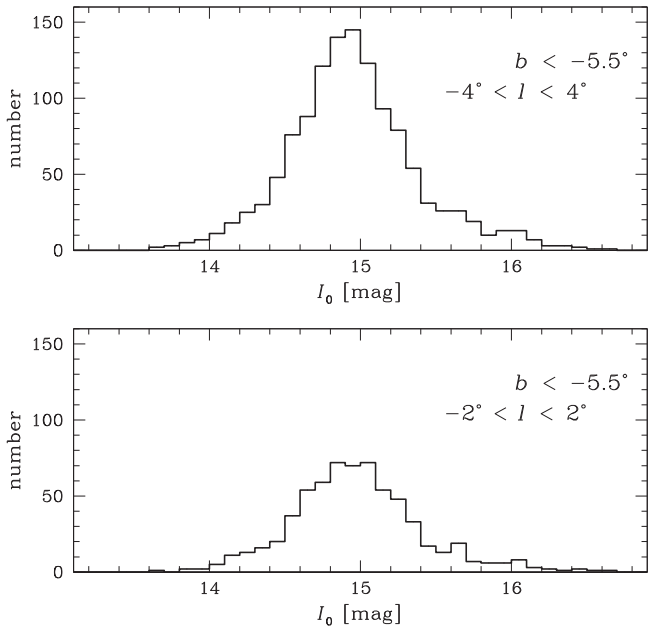


Figure 9. Distributions of the dereddened brightness I_0 for OGLE RRab stars in regions where intermediate-age red clump giants form a prominent X-shaped structure of the Galactic bar. Both distributions are for stars with Galactic latitudes $b < -5.5^\circ$ and around $l = 0^\circ$, but the top distribution is for a range in longitudes that is twice as wide as the bottom one. There is no split in the old bulge traced by RR Lyrae stars.

$-8.5 < b < -5.5$ but with different longitude ranges around $l = 0^\circ$. No split is observed. This confirms that only metal-rich bulge populations have this feature (Ness et al. 2012; Uttenthaler et al. 2012).

5. RADIAL METALLICITY GRADIENT

The well-sampled OGLE light curves of RRab variables allow us to assess metallicities of the stars using the method proposed by Kovács & Zsoldos (1995) and further developed by Jurcsik & Kovács (1996). The iron abundances, which we already derived in the previous section for about 98.5% of stars with a given ϕ_{31} value, are on the Jurcsik (1995) scale. In the top panel of Figure 10, we show the metallicity distribution for 19,869 bulge RRab stars with a measured Galactocentric distance of $r_{\text{GC}} < 4.0$ kpc by binning the data every 0.05 dex. The distribution has a peak at $[\text{Fe}/\text{H}]_{\text{J95}} = -1.02$ dex and a dispersion of 0.25 dex. The same values were reported in Pietrukowicz et al. (2012) for a sample of 10,259 OGLE-III RRab stars. A much larger sample of stars analyzed here allows for verification of a radial metallicity gradient recently noticed by Sans Fuentes & De Ridder (2014). They found it to be very small but relatively significant: -0.016 ± 0.008 dex kpc $^{-1}$. In Figure 11, we plot the metallicity of bulge RRab stars as a function of distance from the GC. We fit linear regression separately to the mean, median, and modal values determined in 0.2 kpc wide bins from 0.3 to 3.3 kpc. The errors of the bin values are weighted by the square root of the number of stars in each bin. In all three cases the obtained gradient is indeed mildly negative but statistically significant ($>4\sigma$). Almost the same slopes for all three measures indicate no change in the shape of the metallicity distribution with distance. A delicate asymmetry of the distribution toward lower metallicities is confirmed in the inequality mode < median < mean at any distance from the center. Constant differences between the

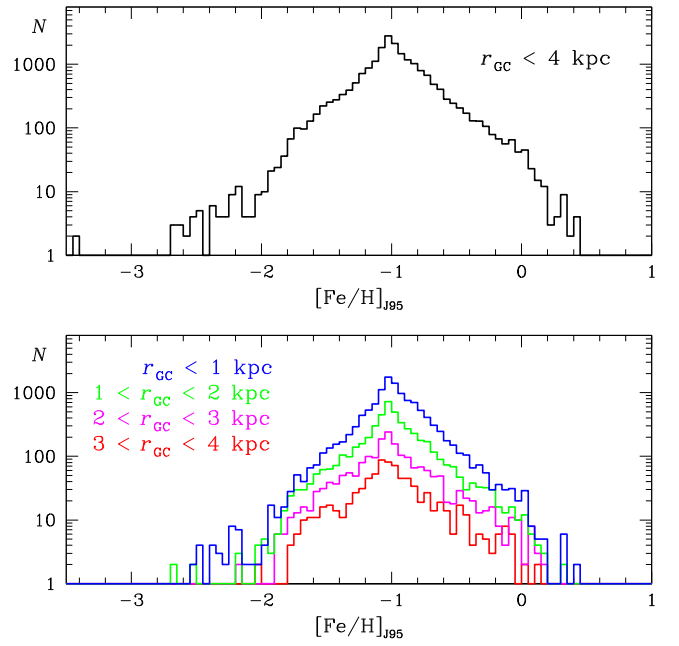


Figure 10. Metallicity distribution on the Jurcsik (1995) scale for all bulge RRab variables with measured Galactocentric distances $r_{\text{GC}} < 4.0$ kpc (top) and for four separate distance ranges (bottom). With increasing distance, the maximum of the distribution slightly moves toward lower metallicities but its shape stays the same.

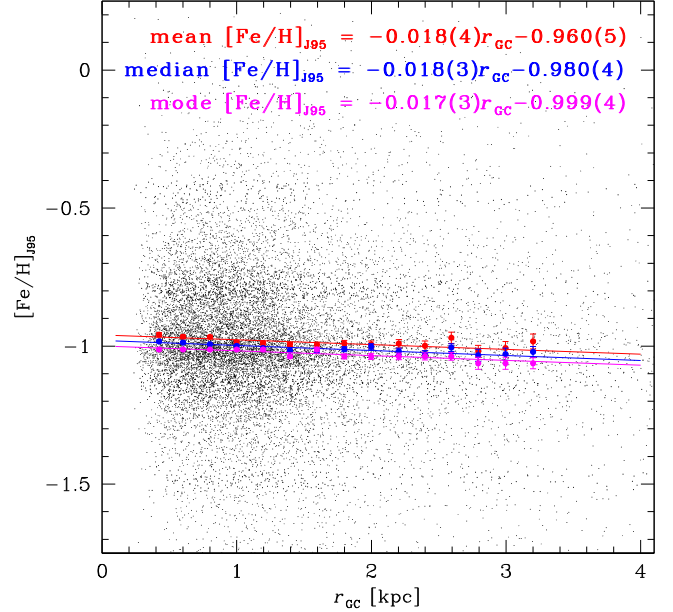


Figure 11. Metallicity as a function of distance from the Galactic center for RRab variables. Relations for average, median, and modal values calculated in 0.2 kpc bins are presented with different colors. The decrease of metallicity with distance is very mild but significant ($>4\sigma$). Almost the same slope for all three relations indicates no changes in the metallicity distribution with distance from the center.

three values indicate no changes in the shape of the distribution with distance. This can also be noted in the bottom panel of Figure 10.

6. MULTIPLE OLD POPULATIONS

Figure 12 presents two period–amplitude (or Bailey) diagrams for OGLE RRab stars, separately for amplitudes in

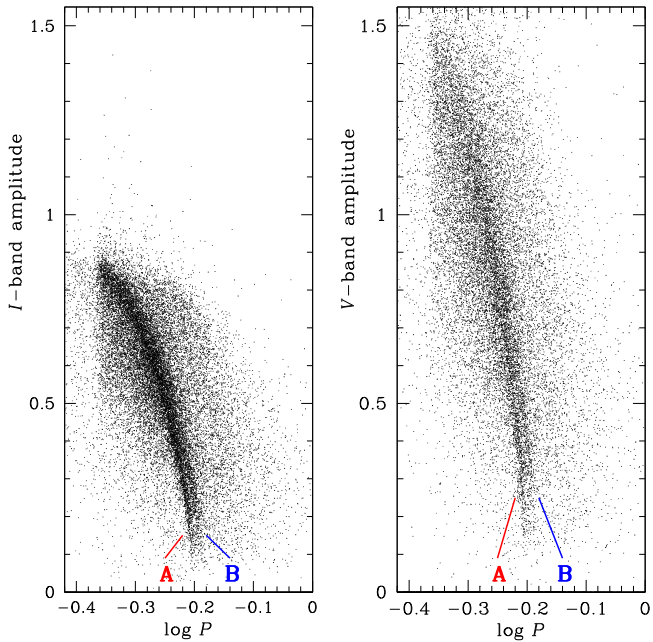


Figure 12. Period–amplitude diagrams for OGLE bulge RRab variables in two observed bands. Two distinct sequences, A and B, are well visible, in particular for low-amplitude stars.

the I band and V band. Surprisingly, the stars form two very close sequences, well resolved at low amplitudes. This is seen even better if we plot only stars with a small scatter around the fit to the I -band data, $\sigma_{\text{fit}} < 0.015$ mag (Figure 13). Such stars constitute about 27% of the original sample of bulge RRab stars. Our interpretation of the period–amplitude diagram is that the two prominent sequences represent two major old bulge populations. We denote the sequence with the shorter periods as population A and the one with the longer ones as population B. The observed separation is much larger than the uncertainty of the period (see plots of σ_P versus $\log P$ and σ_{fit} versus I in Figure 14).

In Figure 15, we analyze the period–amplitude diagram in a quantitative way. First, we have to note that we tried to fit a second-order polynomial (a parabola) to the general trend in the diagram, but it failed. A fourth-order polynomial fits much better to the data for I -band amplitudes < 0.85 mag. We set a central line and nearly parallel boundaries on low and high periods and divided the area between the lines into eight amplitude sectors every 0.1 mag starting from 0.05 mag. In each sector, we counted stars in bins along the trend. The obtained histograms are presented to the right of the period–amplitude diagram in Figure 15. Two peaks are well separated for amplitudes $\lesssim 0.5$ mag. To resolve the two populations at higher amplitudes and find general relations between them we fit a sum of two Gaussians to the data. The fits are presented in the same figure. We can see that the components are significantly different in width and their maxima get closer with increasing amplitude. An average shift between the populations amounts to $\log P = 0.0095(7)$. Population B is about four times more abundant than population A. However, there are many stars beyond the analyzed area, in particular with much shorter periods. They constitute about 40% of the whole sample. Therefore, we conclude that about 12% of RR Lyrae stars belong to population A, about 48% to population B, and the remaining 40% to other populations.

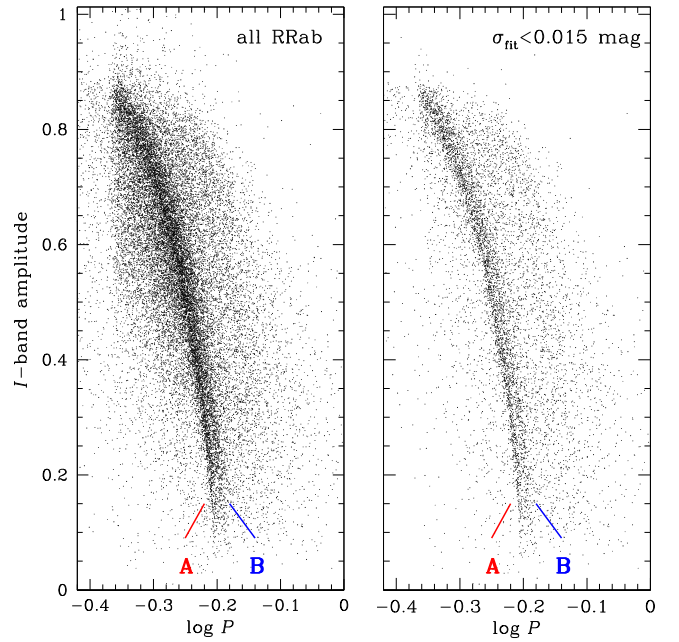


Figure 13. Period–amplitude diagram in the I band for all bulge RRab variables (left panel) and objects with scatter around the fit $\sigma_{\text{fit}} < 0.015$ mag (right panel).

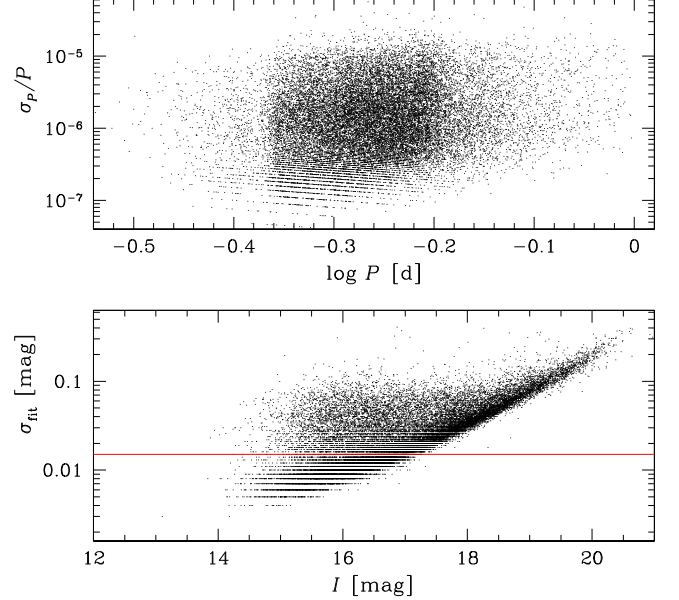


Figure 14. Period uncertainty as a function of period (upper panel) and scatter around the fit as a function of magnitude (lower panel) for all OGLE bulge RRab variables. Stars with $\sigma_{\text{fit}} < 0.015$ mag (below red line) are used in the analysis of the period–amplitude diagram.

By fitting fourth-order polynomials to the points of maxima in the period–amplitude diagram, we find the following relations for the two populations:

$$\begin{aligned} a_{I,\text{popA}} = & -2400(\pm 1100) \log^4 P \\ & - 2800(\pm 1200) \log^3 P - 1290(\pm 500) \log^2 P \\ & - 264(\pm 91) \log P - 20.1(\pm 6.2), \end{aligned} \quad (18)$$

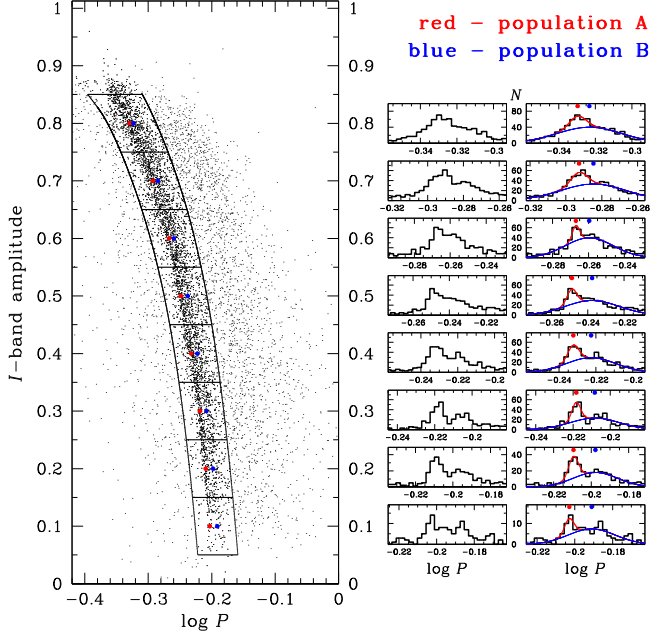


Figure 15. Period–amplitude diagram for bulge RRab variables with $\sigma_{\text{fit}} < 0.015$ mag (on the left-hand side). The presence of two sequences is confirmed on histograms (on the right-hand side) for stars in the marked boxes. Results of the fitting of a sum of two Gaussians are presented in the histograms in the right column. The two components/populations are shown with different colors. The maximum values are marked with points above the histograms and in the boxes in the diagram.

$$\begin{aligned} a_{I,\text{popB}} = & -1740(\pm 740) \log^4 P \\ & - 2040(\pm 810) \log^3 P - 910(\pm 330) \log^2 P \\ & - 184(\pm 58) \log P - 13.9(\pm 3.8). \end{aligned} \quad (19)$$

The two major old bulge populations must have very similar properties since they practically overlap with each other in the period–amplitude diagram. In particular, it is impossible to indicate which variable belongs to which population in a strip along population A. Theoretical (e.g., Bono et al. 1997) as well as empirical investigations (e.g., Fiorentino et al. 2015) on RR Lyrae type variables show that such a split in the Bailey diagram is due to different iron abundance. Based on the present data we can try to search for differences in the metallicity distributions among groups of stars selected in the period–amplitude diagram. In Figure 16, we compare metallicity distributions for stars from a 1σ strip along population A with a 1σ strip along population B. Each strip is actually a mix of populations. The strip along population B contains about 20% of stars from population A, while the strip along population A contains nearly 50% of stars from population B. Nevertheless, the difference in metallicity distributions is noticeable—the one along population A is more skewed toward higher metallicities. In both cases the maximum value is at $[\text{Fe}/\text{H}]_{\text{J95}} = -1.025$ dex, but medians differ by 0.017 dex: -0.947 dex for the strip along population A and -0.964 dex for the one along population B.

In Figure 17, we try to assess the metallicity difference in another way. For each star we calculate the probability of membership in population B and locate the stars in a probability–metallicity diagram. To the formed distribution we fit a straight line. It has $[\text{Fe}/\text{H}]_{\text{J95}} = -0.94$ dex at the end where probability reaches 1 and $[\text{Fe}/\text{H}]_{\text{J95}} = -0.77$ dex where

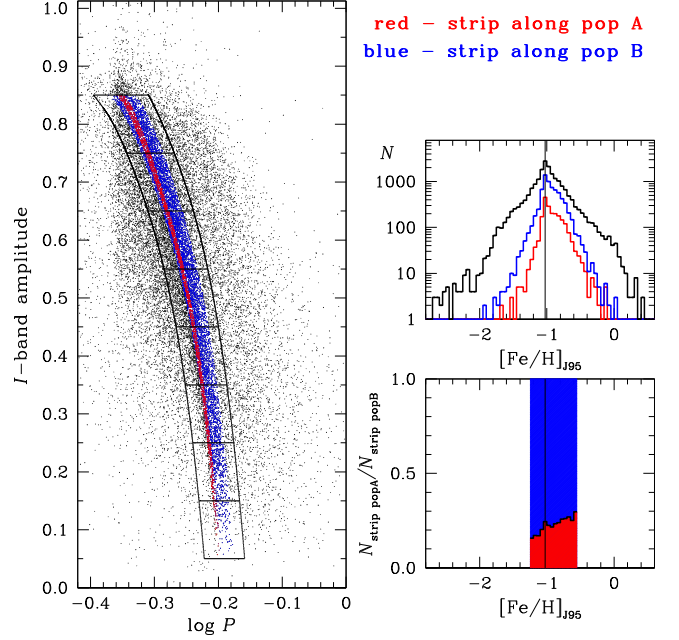


Figure 16. Left panel: period–amplitude diagram for all RRab variables with location of 1σ strips along population A (in red) and population B (in blue). Upper right: histograms of photometrically assessed metallicities on the Jurcsik (1995) scale for all RRab stars (black line), stars from the strip along population A (in red), and stars from the strip along population B (in blue). The bin size is 0.05 dex. The thin vertical line marks the modal value of $[\text{Fe}/\text{H}]_{\text{J95}} = -1.025$ dex. Lower right: normalized proportion of stars from the two strips calculated in the same metallicity bins if the total number of objects exceeds 100 per bin. Note that, despite the same modal value, the distribution of stars from the strip along population A is more skewed toward higher metallicities than the one for stars from the strip along population B.

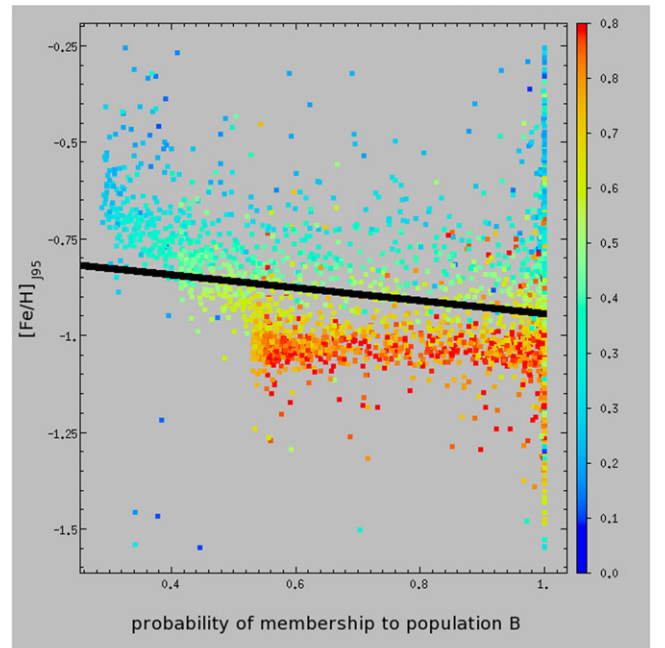


Figure 17. Metallicity distribution in a function of probability that a star belongs to population B. Colors code the I -band amplitude. Inclined black straight line fitted to the data indicates a difference in metallicity of 0.17 dex for the probability from 1 to zero. Population B is clearly more metal-poor than population A and probably by this value.

probability is zero. It is clear again that, on average, stars from population A are richer in metals than stars from population B. The difference of 0.17 dex may be overestimated, but it seems to be a more realistic value than the 0.02 dex derived from the medians.

7. CONCLUSIONS

The recently released collection of 27,258 fundamental-mode RRab type variable stars detected toward the Galactic bulge (Soszyński et al. 2014) by the OGLE survey has been used to study the structure of the old bulge and its properties. The present sample of bulge RRab stars includes newly discovered variables in OGLE-IV and is about twice as large as the one analyzed in Pietrukowicz et al. (2012).

After initial cleaning of the sample from likely globular cluster members and foreground and background objects (mainly from the Sgr dSph galaxy), we investigated the surface density distribution of the bulge RRab stars on the sky. We demonstrated that constant density lines are ellipses flattened along the Galactic equator with a flattening of $f = 0.33 \pm 0.03$. We also found that the density profile can be described by a single power law at observed Galactocentric distances between 0.2 and 2.8 kpc for the distance to the GC of $R_0 = 8.27 \pm 0.01(\text{stat}) \pm 0.40(\text{sys})$ kpc that was obtained in this work.

The analysis of the spatial distribution of RR Lyrae stars shows that they form a triaxial ellipsoid with a major axis located in the Galactic plane and inclined at an angle of $i = 20^\circ \pm 3^\circ$ to the Sun–GC line of sight. This angle is close to the orientation angle of the Galactic bar ($\sim 30^\circ$) traced by intermediate-age RC giants. For the RR Lyrae ellipsoid, we determined the scale-length ratio of the major axis to the minor axis in the plane and to the axis vertical to the plane $1:0.49(2):0.39(2)$. Such a spatial distribution is consistent with the fact that RR Lyrae stars are in the same gravitational potential together with the more massive Galactic bar. The result presented here confirms a conclusion stated in Pietrukowicz et al. (2012) after a comparison of the brightness between the bulge RR Lyrae stars and RC giants in a function of Galactic coordinates, illustrated in their Figures 12–14. The tilt angle of $12.5^\circ \pm 0.5^\circ$ obtained by Dékány et al. (2013) seems to be too small and the metal-poor bulge population indeed trace closely the barred distribution of RC stars. However, we cannot rule out a possibility that the geometric properties of the old bulge are different in its central part.

From the parameters of the *I*-band light curves we assessed metallicities of the bulge RRab stars on the Jurcsik (1995) scale. We confirmed our earlier finding (Pietrukowicz et al. 2012) that the metallicity distribution is sharply peaked at $[\text{Fe}/\text{H}]_{95} = -1.02$ dex, with a dispersion of 0.25 dex. We also confirmed a very weak metallicity gradient with a Galactocentric distance recently noted in Sans Fuentes & De Ridder (2014) based on the OGLE-III data. The analysis of the present sample gives a value of $-0.018(3)$ dex kpc $^{-1}$ and indicates that the shape of the distribution does not change with the distance from the center.

In this work, for the first time, we pay attention to two very close sequences formed by RRab stars in the period–amplitude diagram. We interpret them as the presence of two major old bulge populations, A and B, which differ in their iron content. The mean observed shift between the two populations is 0.0095 (7) in $\log P$, while an estimated difference in metallicity is

about 0.17 dex or lower. We found that population A is about four times less abundant than the slightly more metal-poor population B. By counting stars we have assessed that population A contains about 12% of the bulge RR Lyr stars, populations B about 48%, and other old bulge populations the remaining 40%. The existence of multiple old populations suggests that the early formation of the Milky Way bulge happened via mergers (Kormendy & Kennicutt 2004; Seidel et al. 2010).

The large sample of RR Lyrae stars detected in the optical regime by the OGLE survey has allowed us to study the 3D structure of the old bulge as close as ~ 0.3 kpc from the GC. Soon the ongoing near-IR VVV survey should complete this picture for the most central regions. However, there will still be many questions to answer, in particular, on the assembly history and dynamics of the old bulge and its relation to the Galactic halo. Spectroscopic follow-up observations conducted by surveys such as APOGEE (Nidever et al. 2012) and ARGOS (Freeman et al. 2013) may help us to find answers to these key issues.

The OGLE project has received funding from the National Science Centre, Poland, grant MAESTRO 2014/14/A/ST9/00121 to AU. This work has been also supported by the Polish Ministry of Sciences and Higher Education grants No. IP2012 005672 under the Iuventus Plus program to PP and No. IdP2012 000162 under the Ideas Plus program to IS.

APPENDIX DETERMINATION OF THE c/a RATIO

If we assume that the viewing angle at which we observe the RR Lyr ellipsoid is negligible, the c/a ratio can be estimated from simple geometric considerations. For an ellipsoid with axes a and b in the xy (Galactic) plane and an axis c perpendicular to this plane, we can write:

$$\frac{c}{a} = \frac{c}{y_0} \frac{y_0}{a}, \quad (20)$$

where y_0 is the projected half-width in the plane, as shown in the cross section in Figure 18. In our case c/y_0 roughly equals $r_b/r_l = 1 - f$. The proportion y_0/a can be determined by drawing tangent lines parallel to the inclined ellipse which is a result of the plane cross section of the ellipsoid. The standard equation for the ellipse in the $x'y'$ coordinate system is

$$\frac{x'^2}{a^2} + \frac{y'^2}{b^2} = 1. \quad (21)$$

The $x'y'$ system is rotated with respect to the xy system through the clockwise angle i , hence

$$\frac{(x \cos i + y \sin i)^2}{a^2} + \frac{(x \sin i - y \cos i)^2}{b^2} = 1. \quad (22)$$

Expanding the binomial squares and collecting like terms leads to the following quadratic equation:

$$Ay^2 + By + C = 0, \quad (23)$$

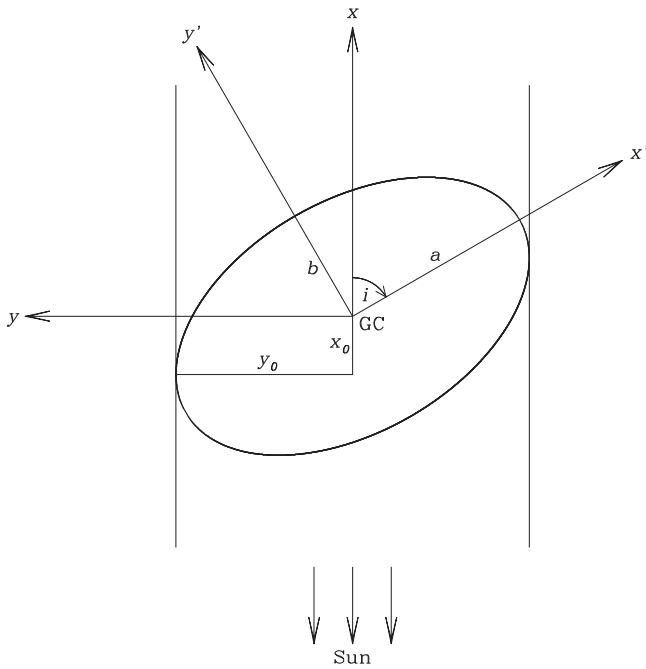


Figure 18. Cross section of an ellipsoid with semiaxes a and b in the Galactic plane and inclined at an angle i to the Sun–GC line of sight.

where

$$A = \frac{\sin^2 i}{a^2} + \frac{\cos^2 i}{b^2},$$

$$B = -2x\left(\frac{1}{b^2} - \frac{1}{a^2}\right)\sin i \cos i,$$

$$C = \left(\frac{\cos^2 i}{a^2} + \frac{\sin^2 i}{b^2}\right)x^2 - 1.$$

The discriminant of the above quadratic equation

$$\Delta = B^2 - 4AC = \frac{4}{a^2 b^2}(b^2 \sin^2 i + a^2 \cos^2 i - x^2). \quad (24)$$

The maximum of the root

$$y = \frac{-B + \sqrt{\Delta}}{2A} \quad (25)$$

is the searched half-width y_0 . From the derivative $dy/dx = 0$, we find

$$\frac{x_0}{a} = \left(1 - \left(\frac{b}{a}\right)^2\right) \sin i \cos i$$

$$\times \sqrt{\frac{\left(\frac{b}{a}\right)^2 \sin^2 i + \cos^2 i}{\left(\frac{b}{a}\right)^2 + \left(1 - \left(\frac{b}{a}\right)^2\right)^2 \sin^2 i \cos^2 i}}. \quad (26)$$

Finally, we obtain

$$\frac{y_0}{a} = \left(\left(1 - \left(\frac{b}{a}\right)^2\right) \frac{x_0}{a} \sin i \cos i + \frac{b}{a} \sqrt{\left(\frac{b}{a}\right)^2 \sin^2 i + \cos^2 i - \left(\frac{x_0}{a}\right)^2} \right) / \left(\left(\frac{b}{a}\right)^2 \sin^2 i + \cos^2 i \right). \quad (27)$$

REFERENCES

- Akhter, S., Da Costa, G. S., Keller, S. C., & Schmidt, B. P. 2012, *ApJ*, **756**, 23
- Bobylev, V. V., Mosenkov, A. V., Bajkova, A. T., & Gontcharov, G. A. 2014, *AstL*, **40**, 86
- Bono, G., Caputo, F., Cassisi, S., Incerti, R., & Marconi, M. 1997, *ApJ*, **483**, 811
- Bono, G., Caputo, F., & di Criscienzo, M. 2007, *A&A*, **476**, 779
- Cao, L., Mao, S., Nataf, D., Rattenbury, N. J., & Gould, A. 2013, *MNRAS*, **434**, 595
- Carretta, E., Bragaglia, A., Gratton, R., D’Orazi, V., & Lucatello, S. 2009, *A&A*, **508**, 695
- Catelan, M. 2004, *ApJ*, **600**, 409
- Catelan, M., Pritzl, B. J., & Smith, H. A. 2004, *ApJS*, **154**, 633
- Chatzopoulos, S., Fritz, T. K., Gerhard, O., et al. 2015, *MNRAS*, **447**, 948
- Clement, C. M., Muzzin, A., Dufton, Q., et al. 2001, *AJ*, **122**, 2587
- Cseresnjes, P. 2001, *A&A*, **375**, 909
- Dékány, I., Minniti, D., Catelan, M., et al. 2013, *ApJL*, **776**, L19
- Drake, A. J., Catelan, M., Djorgovski, S. G., et al. 2013, *ApJ*, **763**, 32
- Fiorentino, G., Bono, G., Monelli, M., et al. 2015, *ApJL*, **798**, L12
- Freeman, K., Ness, M., Wylie-de-Boer, E., et al. 2013, *MNRAS*, **428**, 3660
- Gillessen, S., Eisenhauer, F., Fritz, T. K., et al. 2009, *ApJL*, **707**, L114
- Gonzalez, O. A., Rejkuba, M., Minniti, D., et al. 2011, *A&A*, **534**, L14
- Gonzalez, O. A., Rejkuba, M., Zoccali, M., et al. 2012, *A&A*, **543**, A13
- Hernquist, L. 1990, *ApJ*, **356**, 359
- Jurcsik, J. 1995, *AcA*, **45**, 653
- Jurcsik, J., & Kovács, G. 1996, *A&A*, **312**, 111
- Jurić, M., Ivezić, Ž., Brooks, A., et al. 2008, *ApJ*, **673**, 864
- Keller, S. C., Murphy, S., Prior, S., Da Costa, G., & Schmidt, B. 2008, *ApJ*, **678**, 851
- Kinemuchi, K., Smith, H. A., Woźniak, P. R., & McKay, T. A. 2006, *AJ*, **132**, 1202
- King, I. 1962, *AJ*, **67**, 471
- Kormendy, J., & Kennicutt, R. C., Jr. 2004, *ARA&A*, **42**, 603
- Kovács, G., & Szoldos, E. 1995, *A&A*, **293**, L57
- Kunder, A., & Chaboyer, B. 2009, *AJ*, **137**, 4478
- Marconi, M., Coppola, G., Bono, G., et al. 2015, *ApJ*, **808**, 50
- Mateu, C., Vivas, A. K., Downes, J. J., et al. 2012, *MNRAS*, **427**, 3374
- McWilliam, A., & Zoccali, M. 2010, *ApJ*, **724**, 1491
- Miceli, A., Rest, A., Stubbs, C. W., et al. 2008, *ApJ*, **678**, 865
- Minniti, D., Alcock, C., Alves, D., et al. 1998, in IAU Symp. 184, The Central Regions of the Galaxy and Galaxies, ed. Y. Sofue (Dordrecht: Kluwer), **123**
- Minniti, D., Lucas, P. W., Emerson, J. P., et al. 2010, *NewA*, **15**, 433
- Mizerski, T. 2003, *AcA*, **53**, 307
- Moorthy, B. K., & Holtzman, J. A. 2006, *MNRAS*, **371**, 583
- Morelli, L., Pompei, E., Pizzella, A., et al. 2008, *MNRAS*, **389**, 341
- Nataf, D. M., Gould, A., Fouqué, P., et al. 2013, *ApJ*, **769**, 88
- Nataf, D. M., Udalski, A., Gould, A., Fouqué, P., & Stanek, K. Z. 2010, *ApJL*, **721**, L28
- Ness, M., Freeman, K., Athanassoula, E., et al. 2012, *ApJ*, **756**, 22
- Nidever, D. L., Zasowski, G., Majewski, S. R., et al. 2012, *ApJL*, **755**, L25
- Papadakis, I., Hatzidimitriou, D., Croke, B. F. W., & Papamastorakis, I. 2000, *AJ*, **119**, 851
- Pietrukowicz, P., Udalski, A., Soszyński, I., et al. 2012, *ApJ*, **750**, 169
- Pietrzyński, G., Thompson, I. B., Gieren, W., et al. 2012, *Natur*, **484**, 75
- Rattenbury, N. J., Mao, S., Sumi, T., & Smith, M. C. 2007, *MNRAS*, **378**, 1064
- Reid, M. J., Menten, K. M., Brunthaler, A., et al. 2014, *ApJ*, **783**, 130
- Sandage, A., & Tammann, G. A. 2006, *ARA&A*, **44**, 93
- Sans Fuentes, S. A., & De Ridder, J. 2014, *A&A*, **571**, A59
- Schöenrich, R. 2012, *MNRAS*, **427**, 274
- Seidel, M. K., Cacho, R., Ruiz-Lara, T., et al. 2015, *MNRAS*, **446**, 2837

- Sesar, B., Ivezić, Ž., Grammer, S. H., et al. 2010, *ApJ*, **708**, 717
- Smolec, R., 2005, *AcA*, **55**, 59
- Smolec, R., Pietrzyński, G., Graczyk, D., et al. 2013, *MNRAS*, **428**, 3034
- Soszyński, I., Dziembowski, W. A., Udalski, A., et al. 2011, *AcA*, **61**, 1
- Soszyński, I., Udalski, A., Szymański, M. K., et al. 2014, *AcA*, **64**, 177
- Süveges, M., Sesar, B., Váradí, M., et al. 2012, *MNRAS*, **424**, 2528
- Szczygieł, D. M., Pojmański, G., & Pilecki, B. 2009, *AcA*, **59**, 137
- Torrealba, G., Catelan, M., Drake, A. J., et al. 2015, *MNRAS*, **446**, 2251
- Trager, S. C., Faber, S. M., Worthey, G., & González, J. J. 2000, *AJ*, **120**, 165
- Udalski, A. 2003, *ApJ*, **590**, 284
- Udalski, A., Olech, A., Szymański, M., et al. 1997, *AcA*, **47**, 1
- Udalski, A., Szymański, M., Kaluzny, J., Kubiak, M., & Mateo, M. 1992, *AcA*, **42**, 253
- Udalski, A., Szymański, M., & Szymański, G. 2015, *AcA*, **65**, 1
- Udalski, A., Szymański, M. K., Soszyński, I., & Poleski, R. 2008, *AcA*, **58**, 69
- Uttenthaler, S., Schultheis, M., Nataf, D. M., et al. 2012, *A&A*, **546**, A57
- Wegg, C., & Gerhard, O. 2013, *MNRAS*, **435**, 1874
- Zinn, R., Horowitz, B., Vivas, A. K., et al. 2014, *ApJ*, **781**, 22
- Zinn, R., & West, M. J. 1984, *ApJS*, **55**, 45